




Research Article

Influence of the thermal annealing on the morphological and structural properties of ZnO films deposited onto polyimide substrates by ink-jet printing

O. Dobrozhan¹  · R. Pshenychnyi¹ · S. Vorobiov² · D. Kurbatov¹ · V. Komanicky² · A. Opanasyuk¹

Received: 6 November 2019 / Accepted: 31 January 2020 / Published online: 8 February 2020
© Springer Nature Switzerland AG 2020

Abstract

In this work, ZnO films were deposited onto flexible polyimide substrates by ink-jet printing nanoinks containing polyol-synthesized nanocrystals. ZnO films were annealed at 200–400 °C for 10 min and 60 min under the ambient atmosphere. The morphological (shape, size, size distribution, surface roughness), structural (phase composition, crystal structure), optical (band gap, transmission coefficients) properties and the chemical composition of the synthesized nanocrystals and the obtained films were studied. X-ray diffraction analysis, transmission and scanning electron microscopies, atomic force microscopy, Fourier-transform infrared (FTIR) and optical spectroscopies, and energy-dispersive X-ray spectroscopy (EDS) were used to study the properties of obtained ZnO materials. The films, annealed at $T_a = 400$ °C for $t_a = 60$ min, and nanocrystals, synthesized for $t_g = 120$ min, have the good fundamental characteristics for application in the microelectronic devices, especially in solar cells and thermoelectric generators.

Keywords Flexible films · Zinc oxide · Ink-jet printing · Morphology · Structure · Optical properties

1 Introduction

Up to now, there has been a rapid development of flexible microelectronics devices for that the production process should be low cost, versatile, and scalable as well as such devices should possess transparency with an aim to broad application niche. It can be achieved by the replacement of complex and expensive production techniques (such as lithography and vacuum deposition) to the cheaper and faster printing processes. Among the printing techniques, special attention has been paid to 2D, 3D, and spray deposition techniques. 2D printing is a fast (for example, ordinary office printer allows to deposit 1 m² coating only for 20 min) and zero waste which opens the way to obtain coatings onto flexible substrates with predefined sizes [1–3]. The flexible solar cells, thermoelectric generators, sensors, among others, have already been developed by

applying the 2D printing technique [4–6]. For such devices, that is important to obtain high-quality functional elements, for instance, buffer and window films for solar cells; *n*-type leg for thermoelectric generators; sensitive elements for sensors. For this purpose, ZnO is an important semiconducting material possessing suitable physicochemical properties [7–11]. It should be noted that to carry out 2D printing, there is a need to create functional nanoinks that might be obtained by the formation of printing the suspension of nanomaterials. ZnO nanocrystals for these inks have been synthesized in the polyol solvents [12, 13]. This approach gives an opportunity to control the shape, size, phase, and chemical composition and optical and structural properties of the nanomaterials that, in turn, regulate functional parameters of the final devices. To enhance the working parameters of the described devices,

✉ O. Dobrozhan, dobrozhan.a@gmail.com | ¹Sumy State University, 2, Rymkogo-Korsakova st., Sumy 40007, Ukraine. ²Institute of Physics, P.J. Šafárik University in Košice, 04180 Kosice, Slovakia.



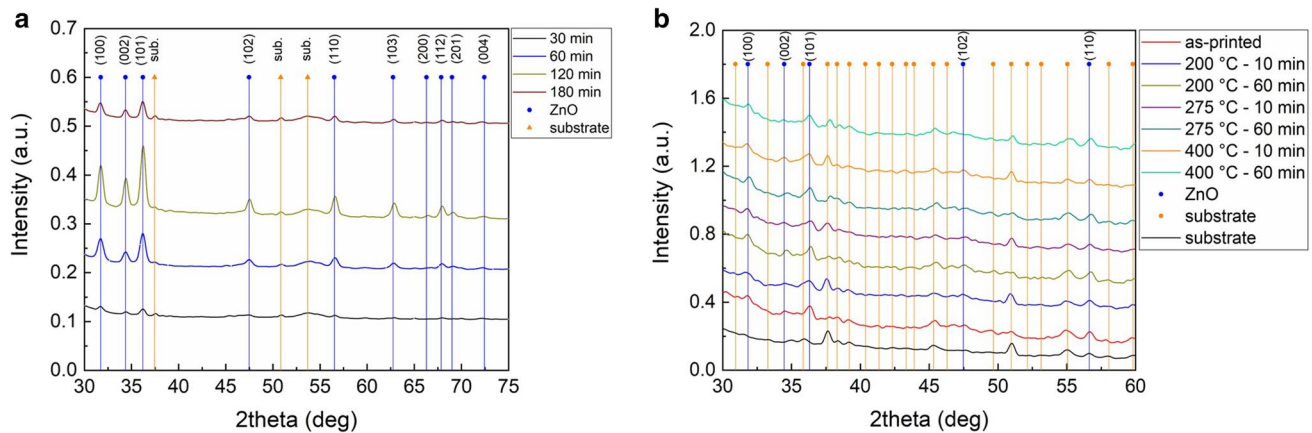


Fig. 1 X-ray diffraction patterns of ZnO nanocrystals at different growth times (orange vertical lines correspond to the polyester substrate, data are taken from [21]; blue vertical lines correspond to ZnO, JCPDS card no. 01-079-2205) (a), and deposited and annealed

ZnO films under the different thermal treatments (orange vertical lines—polyimide substrate, data are taken from [22], blue vertical lines—ZnO, JCPDS card no. 01-079-2205) (b)

ink-jet printed nanocrystalline films can be subjected to thermal and chemical treatments [14].

The fundamental properties of ZnO films have a great impact on working characteristics of thermoelectric generators and solar cells [15, 16]. The single phase of ZnO films helps to reduce the recombination centers inside materials that increase concentration of charge carriers in solar cells. The nanostructuring and surface roughness play important role as these parameters increase number of interfaces and thus improve heterojunction contact in solar cells and scatter phonons to reduce thermal conductivities in thermoelectric generators. The alteration of lattice parameters gives an opportunity to control the cell volume and indicates composition fluctuations that change electrical resistivity, an important property of electronic devices. The control of band gap and transmission parameter allows to control the amount of energy passed through ZnO layer to the absorber layer in solar cells and to engineer electronic structure in thermoelectric material.

Thus, in this work, ZnO films were deposited onto flexible polyimide substrates by 2D ink-jet printing nanoinks containing polyol-mediated nanocrystals. We have studied the growth processes in the nanocrystals depending on the thermodynamic parameter (growth time, t_g) at stabilized kinetic parameters (type and concentration of initial chemical reagents). Furthermore, we have carried out the study of the nanograin growth in the printed films depending on the annealing conditions ($T_a = 200$ °C, 275 °C, 400 °C; $t_a = 10$ min, 60 min). We have defined the effect of nanocrystal growth time, annealing temperature and time of films on the size and shape of nanocrystals, surface roughness, structure and phase composition, chemical nature and bonds, and optical

properties (band gap, E_g , and transmission coefficients, T) of the obtained ZnO materials. To the best of our knowledge, these properties are purely studied for flexible ZnO films deposited by ink-jet printing of nanoinks and further exploration is still required.

2 Experimental details

ZnO nanocrystals were synthesized by polyol method in which a solution of 8.8 g of zinc acetate dihydrate (99%), 40 ml of ethylene glycol (90%), and 1.76 g of polyvinylpyrrolidone (K-25, 90%) were heated to 160 °C with a ramp of 16 °C/min for 180 min. The aliquots were taken at 30 min, 60 min, 120 min, and 180 min of nanocrystal growth. The nanocrystals grown for 120 min were used to obtain printable nanoinks by their dispersion in ethylene glycol with 60 wt% loading. Before printing, the nanoinks were filtered using the membrane filter with a pore size of 450 μ m to remove the nanocrystal agglomerations.

The nanoinks were printed onto ethanol-cleaned polyimide (Kapton) substrates using an office printer Epson TX219 with a piezoelectric sensitive membrane in the printing head. The minimal size of the drop was 4 pl. During the printing process, the highest quality printing mode has been used with the resolution of 5760 \times 1440 dpi. As the substrate, we have used the flexible polyimide films with the sizes of 10 cm \times 10 cm \times 125 μ m. Twenty deposition cycles were applied to grow the films onto a substrate. After the deposition, ZnO films were annealed at $T_a = 200$ °C, 275 °C, 400 °C for $t_a = 10$ min, 60 min.

The morphological properties of nanocrystals and films were studied with an atomic force microscope

(Bruker, ICON), a transmission electron microscope (Selmi, PEM-125 K) and a scanning electron microscope (Tescan, Vega). The chemical composition analysis was carried out using energy-dispersive X-ray spectroscopy (Oxford detector) and a FTIR spectrophotometer (Bruker, Tensor 29). The structural and substructural properties of ZnO nanocrystals and films were determined by the X-ray diffraction method using a DRON-4 device with Cu-K α radiation ($\lambda = 0.15406$ nm) at 40 kV, 20 mA. As a supplement, the selected area diffraction analysis (SAED) technique (TEM 125 K) was applied to identify the phase composition of the samples. The optical properties of ZnO nanocrystals and the obtained ZnO films were studied

using a Solar PB 2201 optical spectrophotometer. The details of methodologies applied to study the structural and optical properties of the samples have been described in our works [17–20].

The optical properties were studied in the range of wavelength $\lambda = (300–900)$ nm. To determine E_g , the absorption coefficient $\alpha(\lambda)$ was calculated from the transmission spectra of ZnO film $T(\lambda)$. The ZnO optical band gap E_g was found from the absorption spectra using the following correlation:

$$\alpha hv = A(hv - E_g)^{1/2}, \quad (1)$$

where α is the absorption coefficient; hv is the photon energy; and A is the constant that depends on the effective mass of the charge carriers in the material. Extrapolation of the linear part of graph $(\alpha hv)^2 - hv$ on energy axis allowed determining the semiconductor band gap E_g .

3 Results and discussion

Figure 1 shows X-ray diffraction patterns of ZnO nanocrystals (a) as well as of the deposited and annealed ZnO films (b). The analysis of the diffraction patterns was performed by comparing the values of angles and intensities on the obtained patterns with the values taken from JCPDS database, card no. 01-079-2205 and other sources [21, 22]. It was found that the synthesized nanocrystals and the obtained films contain a phase of zinc oxide with a hexagonal crystal lattice. Secondary phases were not detected.

It should be noted that the intensity of the lines on diffraction patterns from the nanocrystals increased and their half-widths decreased at a growth temperature of 30–120 min.

At $t_g = 180$ min, the intensity of peaks decreased and the half-width increased, indicating that the nanocrystals first grow and improve their crystalline quality ($t_g = 30–120$ min) and subsequently decrease their size with deterioration of the crystalline quality ($t_g = 180$ min).

The diffraction patterns of ZnO films (Fig. 1b) show the peaks of (100), (002), (101), (102), (110) planes at the angles of $\sim 31.90^\circ$, $\sim 34.47^\circ$, $\sim 36.31^\circ$, $\sim 47.44^\circ$, $\sim 56.67^\circ$, which corresponds to the hexagonal type of ZnO unit lattice.

To determine the influence of growth conditions of nanocrystals and films on its properties, we have determined the following quantitative structural characteristics of ZnO phase: sizes of the coherent scattering domains (L), lattice parameters, and the unit lattice volume (a , c , c/a , V_{unit}). The results are shown in Fig. 2 and in Table 1. As can be seen from Fig. 2a, an increase in the nanocrystal growth time up to 120 min leads to the increase in L values from

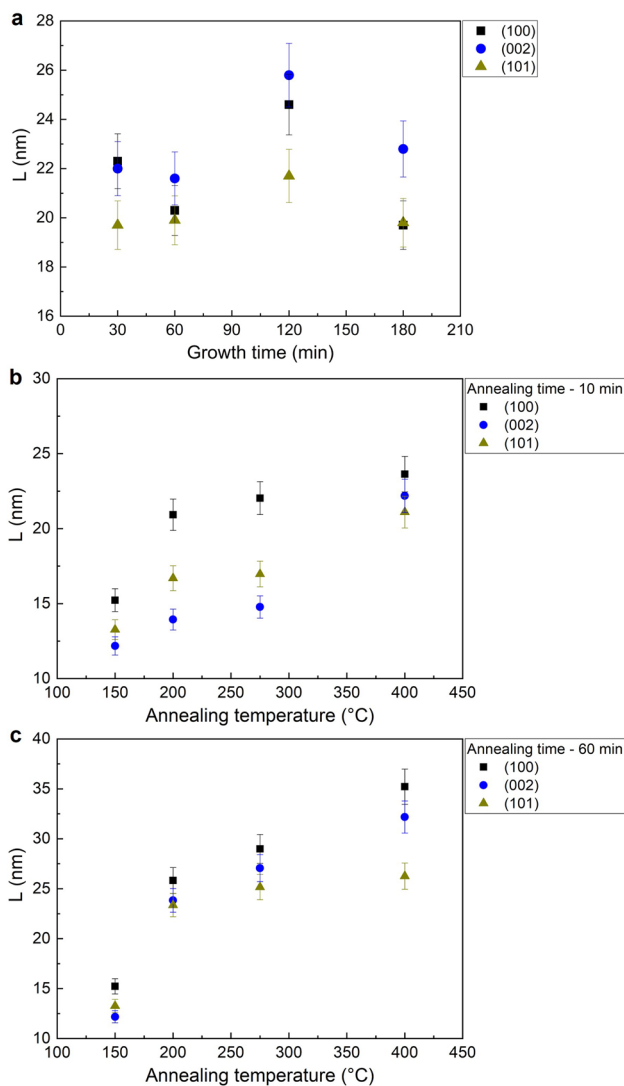


Fig. 2 The influence of nanocrystal growth time (a), temperature and annealing time of films (b, c) on the sizes of coherent scattering domains (L) in the direction perpendicular to the crystallographic (100), (002), (101) planes. The calculation was performed using the Scherrer formula

Table 1 The results of the calculations of the unit lattice parameters (a , c , c/a , V_{unit}) of ZnO materials

| Growth time (min) | 1st iteration | | | 5th iteration | | | V_{unit} (nm ³) |
|----------------------------|---|---------|---------|---------------|---------|--------|--------------------------------------|
| | a | c | c/a | a | c | c/a | |
| 30 | 0.32464 | 0.52156 | 1.6066 | 0.32454 | 0.52186 | 1.6080 | 0.0476 |
| 60 | 0.32476 | 0.52095 | 1.6041 | 0.32472 | 0.52105 | 1.6046 | 0.0476 |
| 120 | 0.32582 | 0.52157 | 1.6008 | 0.32588 | 0.52139 | 1.6000 | 0.0478 |
| 180 | 0.32509 | 0.52199 | 1.6057 | 0.32502 | 0.52221 | 1.6067 | 0.0480 |
| Annealing temperature (°C) | Annealing time, 10 min | | | | | | |
| Deposited films | 0.32411 | 0.52500 | 1.61980 | 0.32375 | 0.52686 | 1.6273 | 0.0478 |
| 200 | 0.32411 | 0.52500 | 1.61980 | 0.32445 | 0.52007 | 1.6029 | 0.0474 |
| 275 | 0.32399 | 0.51898 | 1.60183 | 0.32402 | 0.51886 | 1.6014 | 0.0472 |
| 400 | 0.32372 | 0.51759 | 1.59889 | 0.32381 | 0.51716 | 1.5971 | 0.0469 |
| Annealing temperature (°C) | Annealing time, 60 min | | | | | | |
| Deposited films | 0.32411 | 0.52500 | 1.61980 | 0.32375 | 0.52686 | 1.6273 | 0.0478 |
| 200 | 0.32437 | 0.52069 | 1.60526 | 0.32432 | 0.52094 | 1.6063 | 0.0475 |
| 275 | 0.32453 | 0.52064 | 1.60427 | 0.32450 | 0.52078 | 1.6049 | 0.0475 |
| 400 | 0.32416 | 0.52048 | 1.60564 | 0.32410 | 0.52077 | 1.6068 | 0.0474 |
| Reference | $a=0.32535$ nm; $c=0.52151$ nm; $c/a=1.6029$; $V_{\text{unit}}=0.0478$ nm ³ , JCPDS № 01-080-0074 | | | | | | |

12 to 16 nm in the direction perpendicular to the crystallographic (002) plane. However, with a further increase in t_g up to 180 min, L decreases to 13 nm. Similar trends are observed for the L in the directions perpendicular to (100) and (101) planes. An increase in the annealing temperature of ZnO films to 200–400 °C leads to an increase in the L sizes from 12 to 35 nm. The data analysis shows that the nanocrystals primarily grow in the [001] crystallographic direction.

As can be seen from Table 1, the calculated values of a , c , c/a , and V_{unit} are close to the reference data, which indicates the approximation of the chemical composition of the synthesized nanocrystals and the obtained films to stoichiometric values. It was found that the lattice parameters of ZnO nanocrystals varied in the range of $a_{\text{ZnO}}=(0.32375\text{--}0.32445)$ nm, $c_{\text{ZnO}}=(0.51716\text{--}0.52686)$ nm, and $c/a_{\text{ZnO}}=(1.5971\text{--}1.6273)$. With an increase in nanocrystal growth time, the value of lattice parameter c of zinc oxide increased, while a parameter had the maximum value (closest to the values of the stoichiometric material) at growth time, $t_g = 120$ min. The lattice volume monotonically decreased from $V_{\text{unit}} = 0.0476$ nm³ ($t_g = 30$ min) to $V_{\text{unit}} = 0.0474$ nm³ ($t_g = 180$ min) approaching reference values.

The nanoscale nature and single-phase composition of the synthesized ZnO nanocrystals are confirmed by TEM and SAED analysis (Fig. 3a–d). With increasing crystal growth time, nanocrystal size first increases from 12.0 ± 3.0 nm ($t_g = 30$ min) to 17.3 ± 3.0 nm ($t_g = 120$ min) and then decreases to 12.5 ± 3.0 nm ($t_g = 180$ min).

We attribute such growth behavior to that the nanocrystals enter Ostwald ripening regime at $t_g > 120$ min. The

shape of the nanocrystals was primarily quasispherical. SAED patterns showed that irrespective of the growth time, the synthesized nanocrystals are single-phase supporting XRD data. The nanocrystal sizes determined by TEM studies correlate well with the calculated L values by Scherer formula. The results of SEM and chemical composition studies of ZnO nanocrystals and films are presented in Fig. 4 and Table 2. It was found that both the deposited and annealed films were nanostructured and remained homogeneous after 50 bends in the $10 \times 10 \mu\text{m}$ scanned area. The average film thickness was $1.5 \pm 0.5 \mu\text{m}$. These properties suggest that the obtained ZnO films are suitable for the application in microelectronic devices, especially in solar cells and thermoelectric generators. It should be noted that the synthesized ZnO nanocrystals and the deposited and annealed ZnO films contained an excess of oxygen.

The morphological characteristics of ZnO nanocrystals and films were also investigated using atomic force microscopy. As can be seen from parallel and angle view in Fig. 5, the deposited ZnO films contain nanocrystals in an organic matrix whose volume decreases as the annealing temperature and time of the samples increase. The parameters characterizing the roughness of the sample surfaces are given in Table 2. It should be noted that the values of the arithmetic mean (root mean square) deviation of the surface profile from the median line R_{ms} (R_a) are in nanometer scale, which indicates that the surface of ZnO films is underdeveloped. R_{ms} values increase from 12.1 to 54.1 nm (R_a from 8.9 to 37.9 nm) as the temperature and annealing time increase. This can be explained by the increasing

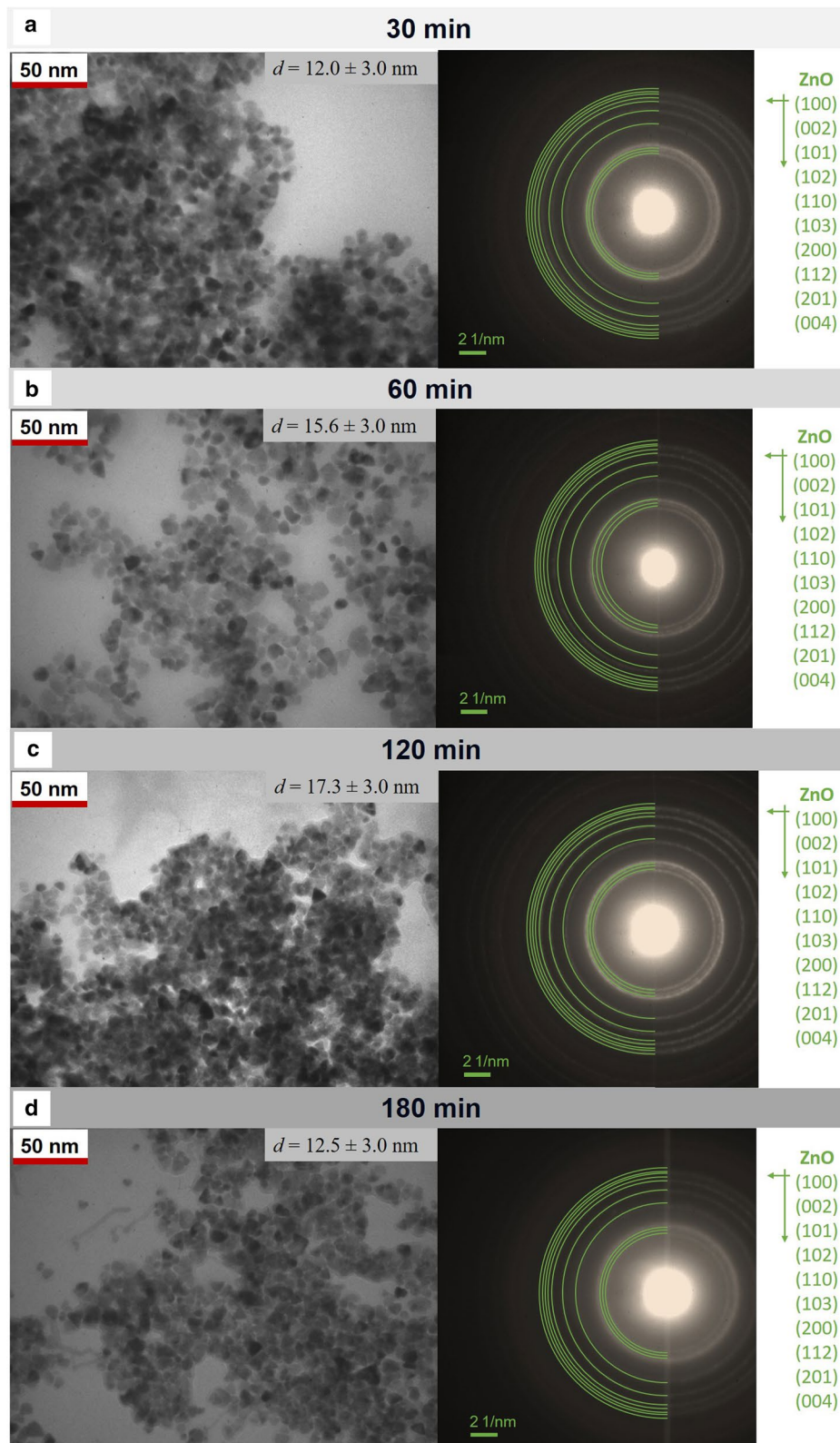


Fig. 3 TEM images and SAED patterns of ZnO nanocrystals synthesized at different times (a-d)

Fig. 4 SEM images of deposited (a) and annealed (b, c) ZnO films and their element mapping (d)

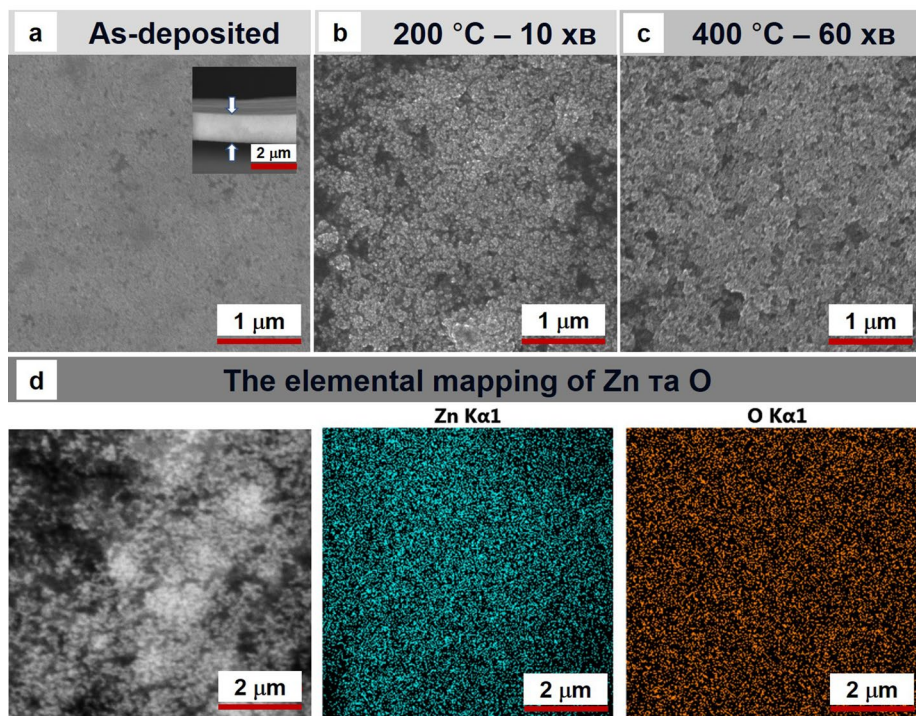


Table 2 Averaged chemical composition, surface roughness, and optical characteristics of ZnO nanocrystals and deposited and annealed ZnO films

| Samples | C_{Zn} , at.% | C_{O} , at.% | $\gamma_{Zn/O}$ | Surface roughness | | E_g , eV | T , % (900 nm) |
|---|-----------------|----------------|-----------------|-------------------|------------|---------------|------------------|
| | | | | R_{ms} (nm) | R_a (nm) | | |
| Nanocrystals | 45.6 | 54.4 | 0.84 | 12.1 | 8.9 | 3.2 ± 0.1 | 60–80 |
| Deposited films | 46.4 | 53.6 | 0.87 | 14.6 | 10.4 | | |
| Annealed films, T_a , °C; t_a , min | | | | | | | |
| 200, 10 | 40.5 | 59.5 | 0.68 | 26.2 | 16.4 | | |
| 200, 60 | 41.3 | 58.7 | 0.70 | 22.5 | 15.8 | | |
| 275, 10 | 41.5 | 58.5 | 0.71 | 30.1 | 22.4 | | |
| 275, 60 | 43.4 | 56.6 | 0.77 | 34.6 | 24.3 | | |
| 400, 10 | 45.8 | 54.2 | 0.85 | 48.4 | 34.2 | | |
| 400, 60 | 45.6 | 54.4 | 0.84 | 54.1 | 37.9 | | |

size of the nanocrystals and the evaporation of the organic matrix material from the film volume.

Increasing the annealing temperature and time allowed to improve the stoichiometry of the films ($\gamma_{Zn/O}$) from 0.68 to 0.84. This can be explained by an increase in the crystallite sizes and the corresponding decrease in the adsorption area of oxygen atoms on nanograins surface as well as by removal of the precursors containing oxygen from the film volume. The element mapping (Fig. 4d) made it possible to establish that zinc and oxygen atoms are distributed uniformly over the film surface. The study of optical characteristics allowed us to determine that the band gap of the materials was $E_g = 3.2 \pm 0.1$ eV, and the transmission coefficients of the films were $T = 60\text{--}80\%$ at 900 nm (Fig. 6).

To detect residual impurities in the nanocrystals and films, FTIR spectra were measured (Fig. 7). The polyimide substrate has been found to contain the following bonding groups: C–N, C–C, CCH–CH₂, C–N + N–H, C–O, CH₂, N–H [23].

The traces of ethylene glycol and water molecules (used in the synthesis process) were found in the synthesized ZnO nanocrystals, as evidenced by the absorption peaks associated with molecular bonds: O–H, C–H, CH₂, C–O–H, C–O, C–C [24]. As can be seen from the figure, the annealed films lead to a significant decrease in the content of organic compounds. It should be noted that such samples still show residues of organic compounds (see chemical bond range up to 2000 cm⁻¹). Such residues are, in our opinion, near the substrate and in the gap between the

Fig. 5 AFM images of deposited (a) and annealed (b–g) ZnO films. The height and surface area were set to 200 nm and 2 × 2 μm, respectively

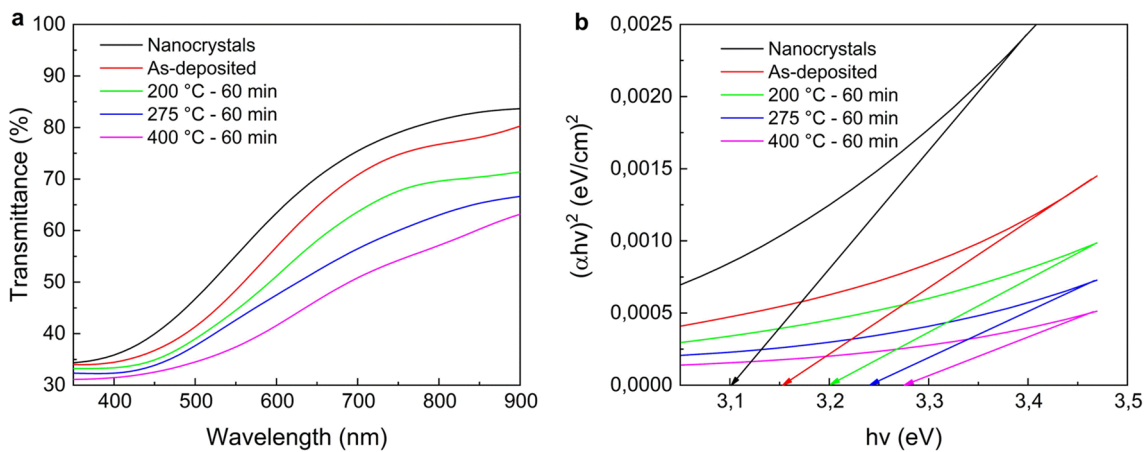
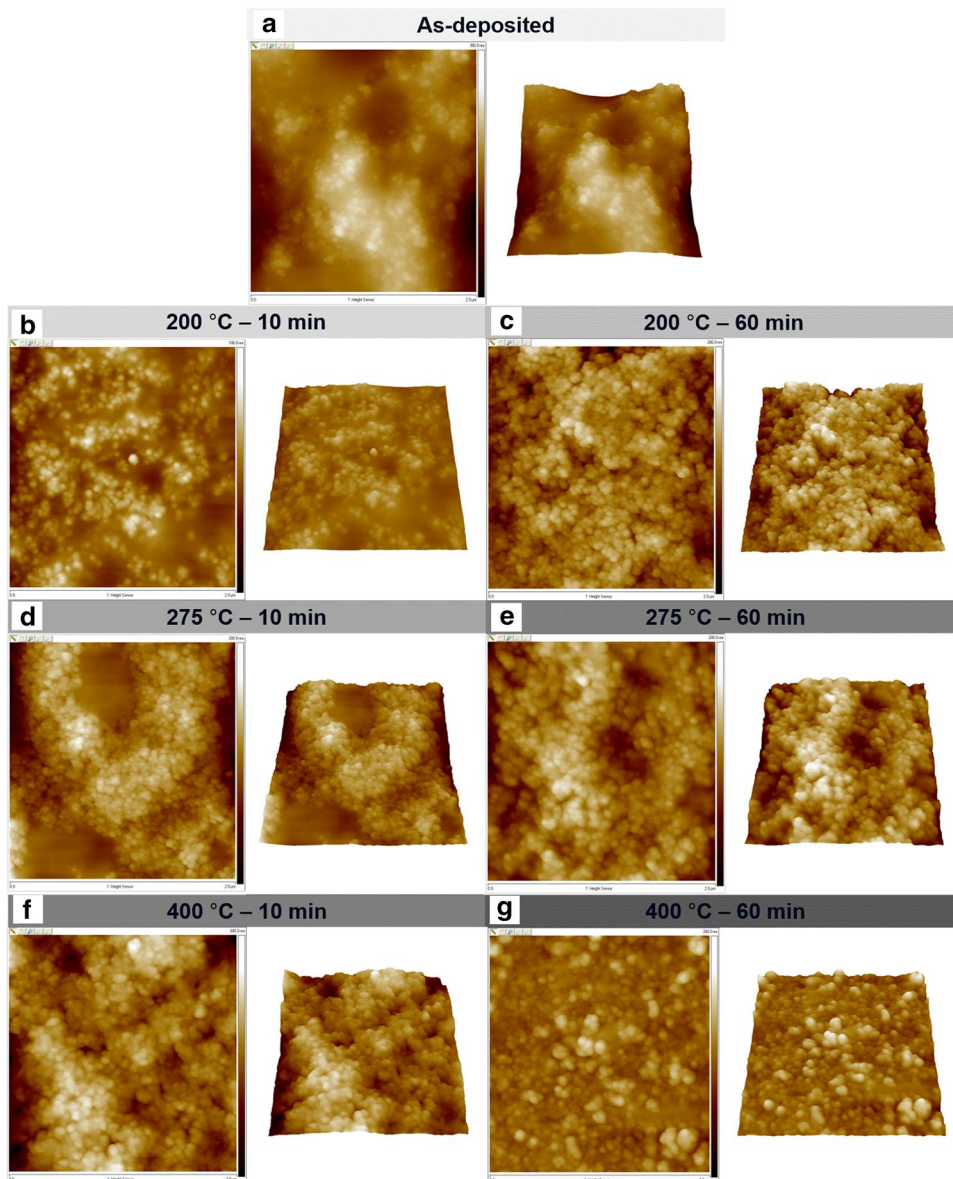


Fig. 6 Transmission coefficients (T) and band gap (E_g) determination images of ZnO nanocrystals, as-deposited and annealed films

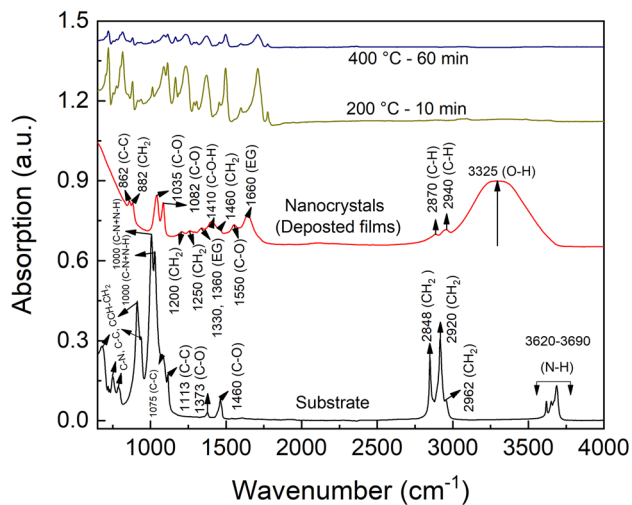


Fig. 7 FTIR spectra of polyimide substrate, ZnO nanocrystals, deposited and annealed ZnO films

crystallites, forming an organic matrix that enhances the adhesion of the film to the substrate surface by forming bonds with polyimide molecular groups. This causes the film to remain intact after temperature annealing and multiple bending of the substrate.

4 Conclusions

In this work, ZnO films were obtained by ink-jet printing of polyol-mediated nanocrystals onto the flexible substrates. The effect of thermal treatments on morphological, structural, and optical properties and the chemical composition of ZnO materials was studied.

The synthesized ZnO nanocrystals were single phase having size of $d = (12.0–17.3) \pm 3$ nm depending on the growth time $t_g = (30–180)$ min. It is shown that the nanocrystals enter the Ostwald ripening regime at $t_g = 120$ min. ZnO films were single phase consisting of nanocrystals distributed in an organic matrix whose content decreased with increasing annealing temperature and time, which was confirmed by the results of AFM microscopy and FTIR spectroscopy.

The lattice parameters of ZnO samples were in the range of $a_{\text{ZnO}} = (0.32375–0.32445)$ nm, $c_{\text{ZnO}} = (0.51716–0.52686)$ nm, and $c/a_{\text{ZnO}} = (1.5971–1.6273)$ and were close to the values of the stoichiometric materials. Structural and substructural characteristics of nanocrystals and films improved with increasing growth and annealing time. ZnO materials were characterized by an excess of oxygen ($\gamma_{\text{Zn/O}} = 0.68–0.84$) in their composition and uniform distribution of chemical elements over the surface. ZnO films were homogeneous with a good adhesion to the substrate

surface having thickness of 1.5 ± 0.5 μm . The films had high optical characteristics (transmission coefficients of $T = 60–80\%$ at 900 nm and band gap of $E_g = 3.2 \pm 0.1$ eV).

The obtained ZnO films possess promising fundamental characteristics for application in flexible microelectronic devices, especially in the solar cells and thermoelectric generators.

Acknowledgements This research was supported by the Ministry of Education and Science of Ukraine (grant numbers: 0116U002619, 0119U100398). The work at Safarik University was supported by grant VEGA no. 1/0204/18, the grant of the Slovak Research and Development Agency under the contract no. APVV-17-0059 and by the ERDF EU Grant under the contract no. ITMS26220120047. We are thankful to Andriy Stepanenko (Department of Electronics, General and Applied Physics, Sumy State University, Sumy, Ukraine) for the measurements and discussion on TEM; to Ihor Shelest (Department of Nanoelectronics, Sumy State University, Sumy, Ukraine) for XRD measurements; to Dr. Matej Baláž (Institute of Geotechnics, Slovak Academy of Sciences, Košice, Slovakia) for FTIR measurements.

Compliance with ethical standards

Conflict of interest The authors declare that they have no conflict of interest.

References

- Nayak L, Mohanty S, Nayak S, Ramadoss A (2019) A review on inkjet printing of nanoparticle inks for flexible electronics. *J Mater Chem C* 7:8771
- Derby B (2015) Additive manufacture of ceramics components by inkjet printing. *Engineering* 1:113
- Gao M, Li L, Song Y (2017) Inkjet printing wearable electronic devices. *J Mater Chem C* 5:2971
- Karunakaran S, Arumugam G, Yang W, Ge S, Khan S, Lin X, Yang G (2019) Recent progress in inkjet-printed solar cells. *J Mater Chem A* 7:13873
- Chen B, Kruse M, Xu B, Tutika R, Zheng W, Bartlett M, Wu Y, Clausen J (2019) Flexible thermoelectric generators with inkjet-printed bismuth telluride nanowires and liquid metal contacts. *Nanoscale* 11:5222
- Ismail M, Hussein A (2017) Enhance the figure of merit for flexible thermoelectric materials by reducing the screening effect. *Appl Nanosci* 7:201
- Wang C, Huang K, Lin D, Liao W, Lin H, Hu Y (2010) A flexible proximity sensor fully fabricated by inkjet printing. *Sensors* 10:5054
- Du Y, Xu J, Paul B, Eklund P (2018) Flexible thermoelectric materials and devices. *Appl Mater Today* 12:366
- Mitra K, Alalawe A, Voigt S, Boeffel C, Baumann R (2018) Manufacturing of all inkjet-printed organic photovoltaic cell arrays and evaluating their suitability for flexible electronics. *Micromachines* 9:642
- Chen X, Li J, Xie Q (2020) Significantly improved photoluminescence properties of ZnO thin films by lithium doping. *Ceram Int* 46:2309
- Li J, Zhu X, Xie Q, Yang D (2019) Surface nanosheets evolution and enhanced photoluminescence properties of Al-doped ZnO

- films induced by excessive doping concentration. *Ceram Int* 45:3871
12. Chieng B, Loo Y (2012) Synthesis of ZnO nanoparticles by modified polyol method. *Mater Lett* 73:78
 13. Mezni A, Kouki F, Romdhane S, Warot-Fonrose B, Joulie S, Mlayah A, Smiri L (2012) Facile synthesis of ZnO nanocrystals in polyol. *Mater Lett* 86:153
 14. Sharma S, Pandeb S, Swaminathan P (2017) Top-down synthesis of zinc oxide based inks for inkjet printing. *RSC Adv* 7:39411
 15. LeBlanc S (2014) Thermoelectric generators: linking material properties and systems engineering for waste heat recovery applications. *Sustain Mater Technol* 1–2:26
 16. Lee TD, Ebong AU (2017) A review of thin film solar cell technologies and challenges. *Renew Sustain Energy Rev* 70:1286
 17. Dobrozhan O, Kurbatov D, Opanasyuk A, Cheong H, Cabot A (2015) Influence of substrate temperature on the structural and optical properties of crystalline ZnO films obtained by pulsed spray pyrolysis. *Surf Interface Anal* 47:601
 18. Nam D, Opanasyuk A, Koval P, Ponomarev G, Ah Jeong G, Kim W, Jo H Cheong (2014) Composition variations in $\text{Cu}_2\text{ZnSnSe}_4$ thin films analyzed by X-ray diffraction, energy dispersive X-ray spectroscopy, particle induced X-ray emission, photoluminescence, and Raman spectroscopy. *Thin Solid Films* 562:109
 19. Dobrozhan O, Opanasyuk A, Kolesnyk M, Demydenko M, Cheong H (2015) Substructural investigations, Raman, and FTIR spectroscopies of nanocrystalline ZnO films deposited by pulsed spray pyrolysis. *Phys Status Solidi A* 212:2915
 20. Ivashchenko M, Buryk I, Opanasyuk A, Nam D, Cheong H, Vaziev J, Bibyk V (2015) Influence of deposition conditions on morphological, structural, optical and electro-physical properties of ZnSe films obtained by close-spaced vacuum sublimation. *Mater Sci Semicond Process* 36:13
 21. Shao D, Wei Q (2018) Microwave-assisted rapid preparation of nano-ZnO/Ag composite functionalized polyester nonwoven membrane for improving its UV shielding and antibacterial properties. *Materials* 11:1412
 22. Shanak H, Ehses K, Gotz W, Pelste L (2009) X-ray diffraction investigations of α -polyamide 6 films: orientation and structural changes upon uni- and biaxial drawing. *J Mater Sci* 44:655
 23. Zarshenas K, Raisi A, Aroujalian A (2015) Surface modification of polyamide composite membranes by corona air plasma for gas separation. *RSC Adv* 5:19760
 24. Krishnan K, Krishnan R (1966) Raman and infrared spectra of ethylene glycol. *Proc Natl Acad Sci India Sect A* 64:111

Publisher's Note Springer Nature remains neutral with regard to jurisdictional claims in published maps and institutional affiliations.